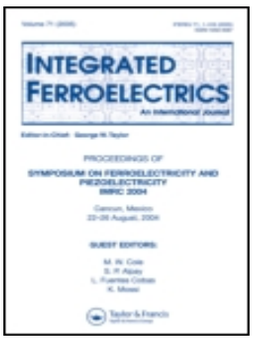

Integrated Ferroelectrics
An International Journal

ISSN: 1058-4587 (Print) 1607-8489 (Online) Journal homepage: http://www.tandfonline.com/loi/ginf20

Structure, Ferroelectric, Dielectric and Energy Storage Studies of $Ba_{0.70}Ca_{0.30}TiO_3$, $Ba(Zr_{0.20}Ti_{0.80})O_3$ Ceramic Capacitors

Venkata Sreenivas Puli, Dhiren K. Pradhan, Brian C. Riggs, Douglas B. Chrisey & Ram. S. Katiyar

To cite this article: Venkata Sreenivas Puli, Dhiren K. Pradhan, Brian C. Riggs, Douglas B. Chrisey & Ram. S. Katiyar (2014) Structure, Ferroelectric, Dielectric and Energy Storage Studies of $Ba_{0.70}Ca_{0.30}TiO_3$, $Ba(Zr_{0.20}Ti_{0.80})O_3$ Ceramic Capacitors, Integrated Ferroelectrics, 157:1, 139-146, DOI: 10.1080/10584587.2014.912939

To link to this article: http://dx.doi.org/10.1080/10584587.2014.912939

Published online: 16 Jun 2014.

Integrated Ferroelectrics, 157:139–146, 2014

ISSN: 1058-4587 print / 1607-8489 online
DOI: 10.1080/10584587.2014.912939

Taylor & Francis
Taylor & Francis Group

Structure, Ferroelectric, Dielectric and Energy Storage Studies of $Ba_{0.70}Ca_{0.30}TiO_3$, $Ba(Zr_{0.20}Ti_{0.80})O_3$ Ceramic Capacitors

VENKATA SREENIVAS PULI,[1,*] DHIREN K. PRADHAN,[2] BRIAN C. RIGGS,[1] DOUGLAS B. CHRISEY,[1] AND RAM. S. KATIYAR[2]

[1]Department of Physics and Engineering Physics, Tulane University, New Orleans, LA 70118, USA
[2]Department of Physics and Institute for Functional Nano Materials, University of Puerto Rico, San Juan, Puerto Rico, PR 00936, USA

$Ba_{0.70}Ca_{0.30}TiO_3$-(BCT),$Ba(Zr_{0.2}Ti_{0.8})O_3$-(BZT) ceramics were fabricated by conventional mixed oxide route to develop inorganic dielectric materials suitable for use as an insulator with high dielectric constant and low energy loss for capacitor applications. The structural phase transition, ferroelectric, dielectric and energy storage properties of BCT, BZT ceramic capacitors were investigated. Room temperature X-ray diffraction (XRD) patterns revealed prominent peaks corresponding to tetragonal perovskite crystal structure for both BCT, BZT solid solutions. Slim ferroelectric hysteresis (P-E) loops were observed for BCT, BZT solid solutions. Temperature dependent dielectric property measurements of BCT, BZT solid solutions have shown a high dielectric constant and low dielectric loss. Room temperature (300K) breakdown field strength and energy densities were obtained from the integral area of P-E loops. For the BCT ceramics, the largest recoverable energy (unreleased energy) density is 1.41 J/cm^3 with dielectric breakdown strength as high as 150 kV/cm. For the BZT ceramics, the largest recoverable energy (unreleased energy) density is 0.71 J/cm^3 with dielectric breakdown strength as high as 150 kV/cm. Bulk BCT, BZT ceramics have shown interesting energy densities; these might be the strong candidate materials for capacitor applications.

Key words Dielectrics; ferroelectrics; energy density; BZT

Introduction

$BaTiO_3$ (BT) is a well known room temperature ferroelectric material and exhibits four phase transitions like cubic paraelectric-tetragonal ferroelectric at 120°C, tetragonal-orthorhombic at 5°C and orthorhombic-rhombohedral at −90°C [1]. Doping, in electroceramics is a common way to improve the material performance [2]. Chemical substitution with either isovalent or aliovalent ions at Ba^{2+} or/and Ti^{4+} site leads to remarkable changes in various characteristics to meet a variety of device applications [3]. Doping with proper

Received September 19, 2013; in final form March 11, 2014.
*Corresponding author. E-mail: pvsri123@gmail.com; vpuli@tulane.edu
Color versions of one or more of the figures in the article can be found online at www.tandfonline.com/ginf.

donor or acceptor impurity ions at either the barium (Ba) or titanium (Ti) site will control the electrical resistance and the ferroelectric Curie temperature (T_c) [4, 5]. Isovalent ion doping (e.g. Sr^{2+} for Ba^{2+}, Zr^{4+} for Ti^{4+}) is often made to shift the Curie temperature (T_c). The magnitude of dielectric constant, ferroelectric phase transition temperature and dielectric tunability of BT can be varied by iso/alio-valent cation doping at the A and B sites and transforms the matrix material into a promising candidate for ferroelectric and piezoelectric applications [6]. Examples of (heterovalent) donor additives are trivalent ion (e.g. La^{3+}, Sb^{3+}) substitution on Ba^{2+} site, or pentavalent ion (e.g. Nb^{5+}, Ta^{5+}) substitution on Ti^{4+} sites of the perovskite ABO_3 lattice [7]. Fe doped $BaTiO_3$ solid solutions are found to exhibit multiferroic properties, however ferroelectric properties of Fe-doped BT are not as pronounced as those of pure BT [8]. Replacing Ba^{2+} by Ca^{2+}, in BT lattice is attracting attention as a superior ceramic capacitor material in which the temperature dependency and reliability of dielectric property of the BT-based materials are improved for electronic applications [9]. Considerable research attention turned towards doping or substitution of isovalent and alio-valent ion for A-site or B-site or both in the BT perovskite crystal lattice structure. Whereas doping at B-site causes Ti^{4+} ion in their TiO_6 octahedra, to displace from the off-center and associated ferroelectric domains are disrupted, which often leads to a broadening of transition at T_c. When the Ti-site is partly replaced with Zr, Hf or Sn, T_c is generally reduced. Introduction of acceptor dopants like Mn at the Ti site in the $BaTiO_3$ lattice, improves the positive temperature coefficient of resistance behavior [10]. Zr is doped into BT at Ti site to reduce dielectric loss at low frequency region [11]. BCT, BZT are among the most studied BT-based solid solution and it has been chosen in capacitor applications. Partial substitution of Ca^{2+} at Ba^{2+} cause a negligible change in the Curie temperature, however there is strong reduction in the tetragonal to orthorhombic phase transition temperature, which leads to improved temperature reliability of tetragonal phase and avoid formation of hexagonal phase. In BZT solid solution, due to presence of chemically more stable Zr^{4+} than Ti^{4+}, this effectively decreases the Curie temperature with better dielectric properties. Here in, we report structural, microstructural, ferroelectric, dielectric and energy storage properties of Ca^{2+}, Zr^{4+} substituted $BaTiO_3$ ceramic capacitors.

Experimental Procedure

Ca and Zr substituted barium titanate (BT): $(Ba_{0.70}Ca_{0.30})TiO_3$-(BCT), $Ba(Zr_{0.2}Ti_{0.8})O_3$-(BZT) solid solutions were prepared by conventional solid state reaction technique. High purity starting powders of $BaCO_3$, TiO_2, and ZrO_2 were mixed with Isopropanol and ball-milled for 4 h at 400 rpm in a planetary ball-mill (Fritsch, Pulverisette500). The powders of the BCT, BZT solid solutions were conventionally calcined at 1250°C for 10 h in an electrical box furnace. Sintering of the BCT pellets was carried out at 1350°C in air for 10 h and BZT pellets was carried out 1500°C in air for 10 h. The X-ray powder diffraction patterns of the pellets were recorded using Cu K_α radiation from a highly stabilized and automated Rigaku X-ray generator operated at 40 kV and 40 mA. Ferroelectric measurements were performed on silver electrode discs (500 μm thickness) with a Radiant Technologies (RT 6000 HVA–4000 V) amplifier. The temperature dependence of the dielectric properties was measured by a HP4284 LCR meter in a computer-controlled MMR technologies K-20 programmer controlled thermal stage. The capacitances of the disks (13 mm diameter and 0.2 cm thickness) were measured as a function of temperature (273–500 K) in a frequency range 100 Hz–100 kHz. Electrical breakdown voltage of the samples was measured at room temperature using Trek high voltage amplifier.

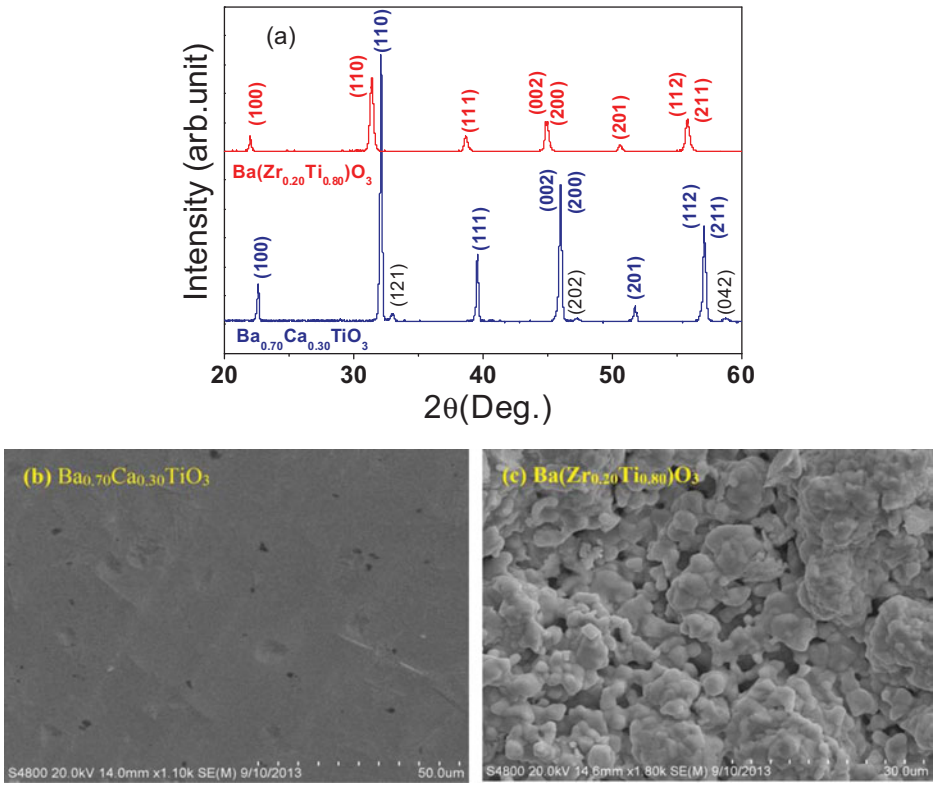

Figure 1. (a) X-ray diffraction patterns and Surface SEM images of (b) $(Ba_{0.70}Ca_{0.30})TiO_3$-(BCT) and (c) $Ba(Zr_{0.2}Ti_{0.8})O_3$-(BZT) ceramics.

Results and Discussion

Structural and Microstructural Studies

Figure 1(a) shows the room temperature XRD patterns obtained from $(Ba_{0.70}Ca_{0.30})TiO_3$ (BCT) ceramics with angle 2θ (degree) ranging from 20° to 60° with a scan rate of 1° per minute. BCT ceramics have shown prominent peaks corresponding to perovskite tetragonal phase and as well extra peaks corresponding to orthorhombic phase were detected. Orthorhombic peaks might be due to solid solubility $x = 0.30$ in BCT lattice. Panigrahi et al., reported that tetragonal and orthorhombic phase coexistence for $Ba_{1-x}Ca_xTiO_3$ ($0.23 < x < 0.90$) [9]. XRD patterns indexed are iso-structural with BCT ceramics (JCPDS 81-1288) [12]. Lattice parameters for BCT ceramics are $a \sim 3.95$ Å, $c \sim 4.06$ Å, tetragonal distortion ($c/a \sim 1.027$) and volume ($\sim$63.70 Å^3). The SEM micrographs of BCT, BZT ceramics are shown in Fig. 1(b, c). It is found that the sintered BCT ceramics are very dense, void free.

The crystalline structure of $Ba(Zr_{0.20}Ti_{0.80})O_3$ (BZT) ceramics were determined by X-ray diffraction technique. Fig. 1(a) shows the room temperature XRD patterns indexed to tetragonal perovskite crystalline structure. XRD patterns revealed that, all the peaks indexed in BZT sintered ceramics had well developed tetragonal perovskite crystalline structure [13]. BZT ceramics sintered at $\sim$1500°C for 6 h could not suppress the extra

peaks, whereas sintering at 1500°C in air for 10 h, revealed pure perovskite crystalline structure.

BZT perovskite phase is characterized mainly by a higher intensity peak (110) at $2\theta = 31.92^{\circ}$. Intense and well-defined diffraction peaks in BZT ceramics indicated a high degree of structural order at long-range. Diffraction angles are little shifted towards higher angle, which might be due to higher amount of Zr content ($x = 0.20$) in the BZT ceramics. Lattice parameter a (~ 4.02) is less than c (~ 4.03), with a tetragonal distortion (c/a) ~ 1.00 and volume ($\sim$65.51 Å^3). It was found that the crystal structure of the ceramics belongs to tetragonal phase but it is close to a cubic phase. The SEM micrographs of BZT ceramics are shown in Fig. 1(c). The microstructure is not completely dense; few scattered pores are observed which indicates that there is certain degree of porosity in the sample. SEM micrographs show the polycrystalline nature of microstructures with different grain size which are inhomogeneously distributed throughout the sample surface. Very dense pore free microstructures with an average grain size around 35–40 μm was observed.

Ferroelectric Studies

The P–E loops were examined using a computer controlled modified Sawyer–Tower circuit operating at a frequency of 50 Hz. BCT ceramics were poled overnight ($\sim$20 kV/cm) and then ferroelectric measurements were carried out. The ferroelectric nature of conventionally prepared BCT ceramics was confirmed by a hysteresis loop of polarization (P) as a function of applied electric field (E) with a maximum electric field of 150 kV/cm. P-E hysteresis loops of the conventionally prepared BCT ceramics were shown in Fig. 2(a). The saturation polarizations (P_s) were ~ 20.22 μC/cm^2, remnant polarization (P_r) ~ 0.99 μC/cm^2 and the coercive field (E_c) ~ 8.15 kV/cm respectively.

Figure 2(a) displays the room temperature P-E hysteresis loops of BZT ceramics (E_{max} $\sim$ 150 kV/cm) measured at 100 Hz. Narrow ferroelectric hysteresis P-E loops are obtained under the maximum electric field (150 kV/cm) before the dielectric breakdown occurs. The ferroelectric nature of conventionally prepared BZT ceramics was confirmed by a hysteresis loop of polarization (P) as a function of applied electric field (E). Similar results were reported for BZT thin films [14]. The long-range polarization ordering due to Ti-O dipole-dipole interaction is hindered, due to higher amounts of Zr^{4+} substitution at Ti^{4+} in $BaTiO_3$ lattice [14]. The saturation polarization (P_s) ~ 14.6 μC/cm^2, remnant polarization (P_r) ~ 2.23 μC/cm^2, coercive field (E_c) $\sim$ 10 kV/cm respectively for of the BZT ceramics were measured. These Polarization values are comparably higher than conventionally prepared $BaZr_{0.20}Ti_{0.80}O_3$ (BZT) ceramics ($P_s \sim 3.5$ μC/cm^2, Pr ~ 0.894 μC/cm^2, Ec $\sim$ 0.4405 kV/cm) [13]. Symmetric nature of butterfly strain–electric-field (S-E) loops suggests the piezoelectric nature of the BCT, BZT ceramics as shown in Fig. 2(b). A maximum strain (S) $\sim$ 5% has been observed for the BCT ceramics and a maximum strain (S) $\sim$ 2% has been observed for BZT ceramics which might be useful in piezoelectric actuator applications. Whereas BCT, BZT strain loops typical "butterfly-shaped" hysteresis loop of a sample with preset polarization can be observed after an initial strain low value, the strain then makes a steep increase until the maximum filed of around 150 kV/cm and then decreased again to a remnant value as the field is released; the same behavior is exhibited for negative polarity field too.

Dielectric Studies

Figure 3(a,b), shows that the temperature dependence of dielectric constant (ε) and dielectric loss (tan δ) measured at different frequencies (100 Hz–1MHz) for BCT,BZT ceramic

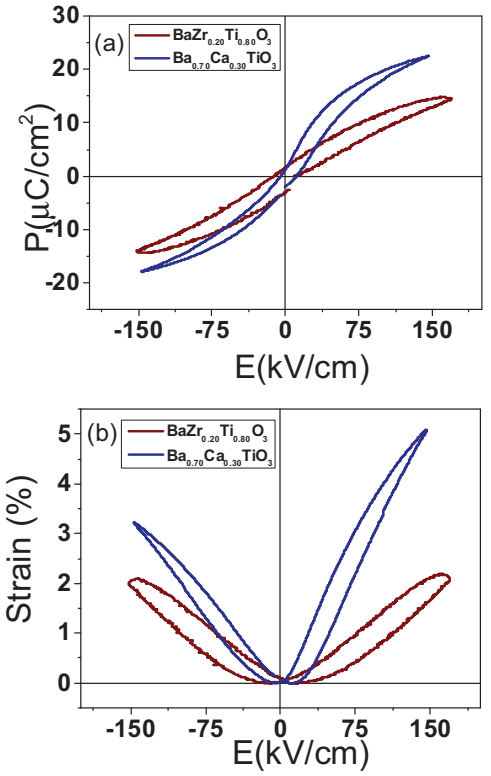

Figure 2. (a) The room temperature P-E loops (b) S-E loops of $Ba_{0.70}Ca_{0.30}TiO_3$-(BCT) and $Ba(Zr_{0.2}Ti_{0.8})O_3$-(BZT) ceramics.

specimens. The dielectric properties of the BCT and BZT ceramics were analyzed in terms of dielectric constant and dielectric loss factor. The variation of dielectric constant and dielectric loss with temperature at different frequencies (Fig. 3) followed the general trend. Dielectric constant decreased with increasing frequency. Temperature dependence of dielectric constant for BCT ceramics at 100 Hz–1MHz, over the temperature range of 273 K to 500 K is displayed in Fig. 3(a). The dielectric constant for BCT ceramics increased up to transition temperature ($T_c \sim 320$ K), and then decreased with increasing temperature. T_c decreased drastically when compared to BCT ceramics ($x \leq 30$) prepared under similar conditions. Decrease in T_c might be attributed to partial substitution of Ca^{2+} at Ti^{4+} site in BCT lattice. Fig. 3(b) shows the temperature dependence of the dielectric loss (tan δ) measured at different frequencies (100 Hz to 1 MHz) for the BCT ceramic specimens. Low dielectric loss (tan $\delta \sim 0.06$–0.012) was recorded at all frequencies (100 Hz–1MHz), throughout the measured temperature range (273 to 500 K) almost constant losses were maintained till 450 K, and thereafter losses were increased. At high temperatures the value of tan δ again increases with rise in temperature. This increasing trend in tan δ in the high temperature and low frequency regions may be due to space charge polarization at the interfaces.

As shown in Fig. 3(c,d) BZT ceramics have shown phase transition corresponding to orthorhombic-tetragonal at (T) $\sim$ 283 K. The high dielectric constant at room temperature for BZT solid solution might be due to the enhanced grain growth which in turn due to the presence of higher ionic radii Zr^{4+} at Ti^{4+} in the $BaTiO_3$ unit cell arises from

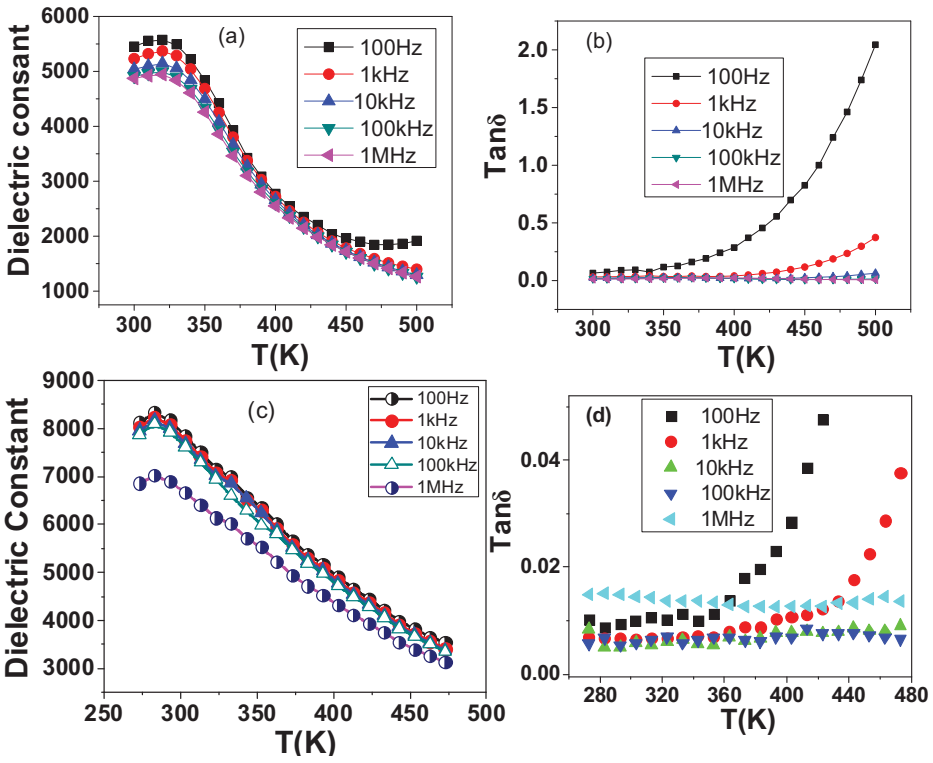

Figure 3. (a) The temperature-dependent dielectric constant (b) dielectric loss of $(Ba_{0.70}Ca_{0.30})TiO_3$-(BCT) (c) The temperature-dependent dielectric constant (d) The temperature-dependent dielectric constant of $Ba(Zr_{0.2}Ti_{0.8})O_3$-(BZT) ceramics.

higher sintering temperature (1500°C). The temperature maxima (T_m) corresponding to the maximum dielectric constant is shifted to lower temperature and the maximum value of dielectric constant is decreased with increasing frequency. A small increase in dielectric constant is observed for initial temperatures up to T = 283 K, where orthorhombic phase is transformed to tetragonal phase. The dielectric constant decreased from $\varepsilon_{max} \sim 2085$ (100 Hz) to $\varepsilon \sim 1741$ (1 MHz) [as shown in Fig. 3(c)]. In the low frequency region the high dielectric constant is observed and as the frequency is increased, the dielectric constant decreased accordingly. An increase in dielectric constant at low frequency and decrease in dielectric constant at high frequency region, with increase in temperature might be due to grain boundary effect and presence of all types of polarizations in the materials.

Figure 3(d) shows the temperature dependence of the dielectric loss (tan δ) measured at different frequencies for the BZT ceramic specimen. Low tan $\delta \sim 0.008$–0.0027 was recorded at all frequencies (100 Hz–1MHz), throughout the measured temperature range (273 to 473 K) almost constant losses were maintained till 400 K, and thereafter losses were increased. The inconsistency in frequency dependence of the dielectric constant and dielectric loss may be due to their different sensitivities to local polarizations, due to appearance of local structural distortion or local polar clusters; the dielectric loss is more sensitive than dielectric constant [15].

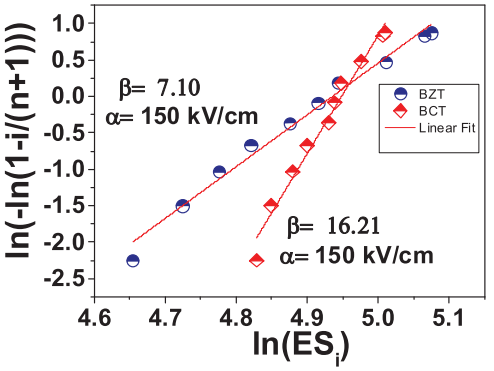

Figure 4. The Weibull distributions and fitting lines of BDS of $(Ba_{0.70}Ca_{0.30})TiO_3$-(BCT), $Ba(Zr_{0.2}Ti_{0.8})O_3$-(BZT) ceramics.

Breakdown Field and Energy Density

Weibull plots are used to interpret failure breakdown analysis of BCT, BZT ceramics. On average minimum 10 ceramics samples were tested for electrical breakdown measurements. Weibull parameters (α, β) were calculated using the relations as mentioned in the reference. Dielectric breakdown field strength (DBS) results (with scale parameter α and shape parameter β) are shown in Fig. 4. In general, Weibull distribution plots show good linearity, however the present BZT ceramics have not shown complete linearity. The X-intercept $\ln(\alpha)$, relates to the magnitude of the breakdown strength; and the shape parameter β, which determines the range of DBS, which is calculated from the slope of the Weibull plots. From the Weibull distribution fitting plots for BCT and BZT were [$\beta \sim 16.21$, $\alpha \sim$ 150 kv/cm] ~7.10 ($\alpha \sim$ 150kv/cm) respectively.

Charge, discharge curve energy storage densities were investigated in terms of ferroelectric polarization-electric field (P-E) hysteresis loops. Charge and discharge curve energy densities were calculated from integral area of P-E loops at room temperature. The energy density is the integral area of the P-E loop (charge-lower branch of P-E curve or discharged curve-upper branch of P-E curve) and y-axis is given by $E_d = \int E.dP$, here E is applied electric field and P is polarization. The ratio of discharge energy density $(Ed)_d$ to that of the charge energy density $(Ed)_c$ can be used to evaluate the energy efficient $[\eta = (Ed)_d / (Ed)_c]$ and to analyze the energy storage mechanism of the dielectric materials. Discharge curve energy density and charge curve energy density of BCT ceramics were 1.41 J/cm^3, 2.28 J/cm^3 with energy efficiency $\eta \sim 61\%$ and discharge curve energy density and charge curve energy density of BZT ceramics were 0.71 J/cm^3, 3.75 J/cm^3 with energy efficiency $\eta \sim 19\%$ respectively. Higher value of discharge energy density or recoverable energy density might be due to large difference between saturation polarization (P_s) and remnant polarization (P_r) and the high breakdown field strength. In the present BCT, BZT ceramics, the large difference between (P_s- P_r) ~ 19.23 μC/cm^2, 12.37 μC/cm^2 respectively.

Conclusions

We investigated the structure, ferroelectric, piezoelectric, dielectric and energy storage properties of $Ba_{0.70}Ca_{0.30}TiO_3$-(BCT),$Ba(Zr_{0.2}Ti_{0.8})O_3$ (BZT) ceramics prepared by solid state sintering method. BCT, BZT ceramics have shown tetragonal perovskite crystal structure at

room temperature in $BaTiO_3$ lattice. Slim ferroelectric P-E hysteresis loops were obtained both BCT, BZT ceramics at a maximum breakdown field of 150 kV/cm with energy density as high as 1.21 J/cm^3, 0.71 J/cm^3. Bulk BCT, BZT ceramics with ferroelectric and piezoelectric behavior might be useful in actuator applications. Uniform dense microstructure might be the reason for high energy storage capability of BCT ceramics, when compared to porous BZT ceramics. Optimizing intrinsic and extrinsic parameters (composition, bulk structure defect chemistry, microstructural development, thickness, electrode configuration and grain size and) will further improve dielectric breakdown values and enhance energy densities in making commercially viable energy storage device capacitors for wide range of energy storage applications.

Funding

This work was supported by the NSF-EFRI Award # 1038272 grant.

References

1. V. S. Puli, A. K. Douglas, B. Chrisey, M. Tomozawa, J. F. Scott, and R. S. Katiyar, *J. Phys. D: Appl Phys*. **44**, 395403–395413 (2011).
2. Z. Yu, C. A. Ruyan Guo, and A. S. Bhalla, *Mat. Lett.* **61**, 326–329 (2007).
3. S. Mahajan, O. P. Thakur, K. Sreenivas, and C. Prakash, *Integr. Ferro*. **122**, 83–89 (2010).
4. A. Dixit, S. B. Majumder, P. S. Dobal, R. S. Katiyar, and A. S. Bhalla, *Thin Solid Films* **447–448**, 284–288 (2004).
5. P. S. Dobal, A. Dixit, R. S. Katiyar, Z. Yu, R. Guo, and A. S. Bhalla, *J.Appl. Phys.* **89**[12], 8085–8091 (2001).
6. W. Liu and X. Ren, *Phys. Rev. Lett.* **103**, 257602 (2009).
7. P. Bomlai, N. Sirikulrat, A. Brown, and S. J. Milne, *J. Euro. Ceram. Soc.* **25**, 1905–1918 (2005).
8. V. S. Puli, I. Coondoo, N. Panwar, A. Srinivas, and R. S. Katiyar, *J.Appl. Phys.* **111**, 102802 (2012).
9. M. R. Panigrahi and S. Panigrahi, *Physica B* **405**, 1787–1791 (2010).
10. A. Belous, O. V'yunov, and L. Kovalenko, *Mat. Res. Bull.* **39**, 297–308 (2004).
11. W. Cai, C. Fu, J. Gao, Z. Lin, and X. Deng, *Ceram. Int.* **38**, 3367–3375 (2012).
12. C.-X. Li, B. Yang, S.-T. Zhang, R. Zhang, Y. Sun, J.-J. Wang, R.-X. Wang, and W. Cao, *Ceram. Int.*, http://dx.doi.org/10.1016/j.ceram.int.2013.04.052 (2013).
13. W. Cai, C. Fu, J. Gao, and X. Deng, *J. Mat. Sci.: Mat. Elect.* **21**, 796–803 (2010).
14. A. Dixit, S. B. Majumder, R. S. Katiyar, and A. S. Bhalla, *J. Mat. Sci.* **41**, 87–96 (2006).
15. Z. Yu, R. Guo, and A. S. Bhalla, *J. Appl. Phys.* **88**, 410 (2000).